EurJChem European Journal of Chemistry
ATLANTA PUBLISHING HOUSE

Check for updates
View Journal Online
View Article Online

Synthesis, X-ray crystal structure, Hirshfeld surface analysis, and molecular docking studies of DMSO/H_2O solvate of 5-chlorospiro[indoline-3,7'-pyrano[3,2-c:5,6-c']dichromene]-2,6',8'-trione

Varun Sharma [1], Bubun Banerjee [2], Aditi Sharma [2] and Vivek Kumar Gupta [1,*]

[1] *Department of Physics, University of Jammu, Jammu Tawi-180006, India*
varunsharma5228@gmail.com (V.S.), vivek.gupta2k9@gmail.com (V.K.G.)
[2] *Department of Chemistry, Akal University, Talwandi Sabo, Bathinda, Punjab-151302, India*
banerjeebubun@gmail.com (B.B.), aditi2195sharma@gmail.com (A.S.)

* *Corresponding author at: Department of Physics, University of Jammu, Jammu Tawi-180006, India.*
e-mail: vivek.gupta2k9@gmail.com (V.K. Gupta).

RESEARCH ARTICLE

10.5155/eurjchem.12.4.382-388.2141

Received: 08 July 2021
Received in revised form: 11 August 2021
Accepted: 28 August 2021
Published online: 31 December 2021
Printed: 31 December 2021

KEYWORDS

Indoline
Mandelic acid
Direct methods
Hydrogen bonding
X-ray crystallography
Hirshfeld surface analysis

ABSTRACT

The title compound, 5-chlorospiro[indoline-3,7'-pyrano[3,2-c:5,6-c']dichromene]-2,6',8'-trione was synthesized *via* one-pot pseudo three-component reaction between one equivalent of 5-chloroisatin and two equivalents of 4-hydroxycoumarin using mandelic acid as catalyst in aqueous ethanol at 110 °C. The synthesized compound was characterized by FT-IR, ^1H NMR, and HRMS techniques. Single crystals were grown for crystal structure determination by using single X-ray crystallography technique. It was found that the crystals are triclinic with space group *P*-1 and Z = 1. The crystal structure was solved by direct method and refined by full-matrix least-squares procedures to a final R-value of 0.0688 for 6738 observed reflections. The crystal structure was stabilized by elaborate system of O-H···O, N-H···O, and C-H···O interactions with the formation of supramolecular structures. 3D Hirshfeld surfaces and allied 2D fingerprint plots were analyzed for molecular interactions. Molecular docking studies have been performed to get insights into the inhibition property of this molecule for Human topoisomerase IIα.

Cite this: *Eur. J. Chem.* **2021**, *12(4)*, 382-388 **Journal website**: www.eurjchem.com

1. Introduction

In many occasions, spiroheterocycles are found to possess a wide range of biological activities [1]. Among many others, spirooxindoles are regarded as one of the important classes of spiroheterocycles [2,3]. Additionally, various scaffolds bearing 4-hydroxycoumarin moiety are also showed significant biological efficacies [4]. Isatin itself possesses so many biological activities [5]. In 2016, Parthasarathy *et al*. [6] synthesized a series of spirooxindole[pyrano-*bis*-2*H*-l-benzopyran] derivatives which showed excellent antimicrobial activity. Very recently, we have reported the synthesis and crystal structure of 5-bromospiro[indoline-3, 7'-pyrano[3, 2-*c*:5, 6-*c*']dechromene]-2,6',8'-trione [7]. During last two decades, organo-catalyzed reactions have been gaining tremendous attention to design sustainable protocols [8-14]. In continuation of our continued interest in mandelic acid catalyzed reactions [15-18], in this communication, we want to report mandelic acid catalyzed synthesis, X-ray structure, Hirshfeld surface analysis and molecular docking studies directing us to investigate the potential anticancer quality of a spirooxindole[pyrano-*bis*-2*H*-l-benzopyran] derivative, namely 5-chlorospiro[indoline-3,7'-pyrano[3,2-*c*:5,6-*c*']dichromene]-2,6',8'-trione (**I**). The title compound was synthesized *via* one-pot pseudo three-component reaction between one equivalent of 5-chloroisatin (**A**) and two equivalents of 4-hydroxycoumarin (**B**) using commercially available mandelic acid as an inexpensive, naturally occurring, environmentally benign organo-catalyst in aqueous ethanol under reflux conditions at 110 °C. Mandelic acid activates the carbonyl group of isatin (present at the C-3 position) which eventually facilitate the attack by the 4-hydroxycoumarin.

2. Experimental

2.1. Synthesis

To an oven-dried round bottom flask, 5-chloroisatin (0.180 g, 1 mmol), 4-hydroxycoumarin (0.324 g, 2 mmol), mandelic acid (0.031 g, 20 mol %) and 5 mL aqueous ethanol (EtOH:H_2O, 1:1, v:v) were added sequentially. The reaction mixture was then allowed to reflux for five hours at 110 °C (Scheme 1).

ISSN 2153-2249 (Print) / ISSN 2153-2257 (Online)
https://dx.doi.org/10.5155/eurjchem.12.4.382-388.2141

Table 1. Crystallographic characteristics, details of X-ray data collection, and structure refinement parameters for compound **I**.

Empirical formula	$C_{108}H_{64}Cl_4N_4O_{29}S_2$
Formula weight	2087.55
Temperature (K)	149.99(10)
Crystal system	Triclinic
Space group	*P*-1
a (Å)	11.8182(6)
b (Å)	12.7608(11)
c (Å)	17.1455(11)
α (°)	77.158(6)
β (°)	73.729(5)
γ (°)	66.373(7)
Volume (Å^3)	2256.2(3)
Z	1
ρ_{calc} (g/cm^3)	1.536
μ (mm^{-1})	0.269
F(000)	1072.0
Crystal size (mm^3)	0.3 × 0.2 × 0.2
Radiation	MoKα (λ = 0.71073)
2Θ range for data collection (°)	3.512 to 50
Index ranges	$-14 \le h \le 14, -15 \le k \le 14, -19 \le l \le 20$
Reflections collected	11884
Independent reflections	7896 [R_{int} = 0.0230, R_{sigma} = 0.0451]
Data/restraints/parameters	7896/38/730
Goodness-of-fit on F^2	1.249
Final R indexes [I≥2σ (I)]	R_1 = 0.0688, wR_2 = 0.1389
Final R indexes [all data]	R_1 = 0.0797, wR_2 = 0.1438
Largest diff. peak/hole (e Å^{-3})	0.29/-0.41

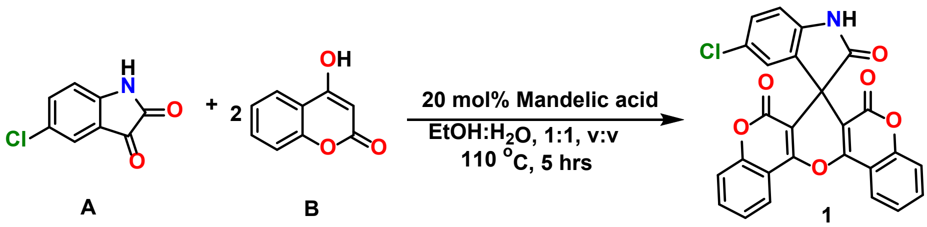

Scheme 1. Mandelic acid catalysed synthesis of 5-chlorospiro[indoline-3,7'-pyrano[3,2-c:5,6-c']dichromene]-2,6',8'-trione.

The progress of the reaction was monitored by TLC. On cooling at room temperature, a solid mass was precipitated out and that was filtered off. The crude residue was further purified by column chromatography. For crystallization, 0.032 g of the purified compound was dissolved in 3 mL DMSO and left at room temperature. White block-shaped crystals 5-chloro spiro[indoline-3, 7'-pyrano[3, 2-*c*:5, 6-*c*']dichromene]-2, 6', 8'-trione (**I**)were obtained after almost ten days. Single crystal was obtained from ethanol as solvent. For crystallization, 0.025 g of the purified compound was dissolved in 3 mL DMSO and left at room temperature. Orange block shaped crystals were obtained after a few days.

5-Chlorospiro[indoline-3, 7'-pyrano[3, 2-*C*:5, 6-*C*']dechro mene]-2,6',8'-trione (**I**): Color: White. Yield: 57%. M.p.: 182-183 °C. FT-IR (KBr, ν, cm^{-1}): 3384 (NH), 1715 (C=O) (ester), 1654(C=O) (ester), 1621 (C=O) (amide). ^{1}H NMR (400 MHz, DMSO-d_6, δ, ppm): 11.01 (brs, 1H, -NH), 8.43 (d, 2H, *J* = 8.0 Hz, Ar-H), 7.88-7.83 (m, 2H, Ar-H), 7.63-7.54 (m, 3H, Ar-H), 7.47 (d, 2H, *J* = 8.0 Hz, Ar-H),7.36 (d, 1H, *J* = 8.0 Hz, Ar-H), 6.77 (d, 1H, *J* = 7.8 Hz, Ar-H). ^{13}C NMR (100 MHz, DMSO-d_6, δ, ppm): 176.12, 156.17, 156.06, 153.89 (2C), 152.08 (2C), 143.54, 134.04 (2C), 131.73 (2C), 127.36 (2C), 124.97 (2C), 123.74 (2C), 116.57 (2C), 113.12, 113.03, 110.74 (2C), 103.09, 46.52. HRMS (ESI-TOF, *m/z*) calcd. for $C_{26}H_{12}ClNO_6$, 469.0353; found 469.0513.

2.2. Crystal structure determination and refinement

The molecular structure solution was obtained by direct method procedure as using SHELXT [19]. The structure was solved by direct methods. Eleven cycles of full-matrix least-squares refinement was carried out and it brought the final R-factor to 0.0688 for 6738 reflections. All non-hydrogen atoms of the molecule were located in the best E-map and refined in anisotropic approximation using SHELXS [19]. All hydrogen atoms were geometrically fixed and a riding model was used for them (N–H = 0.86, C–H = 0.93-0.98 Å), U_{iso}(H) = 1.5U_{eq} for the attached C atoms of methyl groups and 1.2U_{eq}(N,C) for other H atoms except for H11, H20, H23, H53, and H57 of main molecules and H92C, H93B, H93D, H93E, H92G, H92H, H93H, and H93G atoms of solvent molecules. They were localized from the difference Fourier map, and their parameters were refined in the isotropic approximation of atomic displacements. The geometry of the molecule was calculated using the WinGX [20], PARST [21], and PLATON [22] programs. The crystallographic data are summarized in Table 1. Hirshfeld surfaces are mapped using d_{norm}, the shape index, curvature and 2D fingerprint plots presented in this paper were generated using Crystal Explorer 17 [23].

2.3. Molecular docking studies

Molecular docking was carried out using Autodock Vina to find the binding energy and interactions of synthesized molecule **I** to the binding pocket of target protein Human topoisomerase IIα (PDB ID: 1ZXM) at 1.87 Å resolution as co-crystal, downloaded from the Protein Data Bank (http://www.rcsb.org) [24]. After docking, the results were visualized using Discovery Studio [25].

3. Results and discussion

3.1. X-ray structure analysis

The molecular structure containing atomic labeling of the asymmetric unit of crystal **I** “4($C_{26}H_{12}ClNO_6$)·2(C_2H_6OS)·2(H_2O).0” is shown in Figure 1 [26].

Table 2. Selected bond lengths and angles for compound **I**.

Bond	***d*, Å**	**Bond**	***d*, Å**
C1-O2	1.379(5)	C37-O36	1.382(5)
C3-O2	1.382(5)	C35-O36	1.374(5)
C3-O34	1.215(5)	C37-O68	1.202(5)
C7-O33	1.212(5)	C41-O67	1.202(5)
C7-O8	1.375(5)	C41-O42	1.376(5)
C9-O8	1.378(5)	C43-O42	1.383(5)
C15-O16	1.365(5)	C49-O50	1.372(4)
C17-O16	1.371(5)	C51-O50	1.364(5)
C24-N23	1.393(5)	C58-N57	1.366(5)
C30-N23	1.360(5)	C64-N57	1.393(5)
C27-Cl32	1.743(4)	C61-Cl66	1.749(4)
C30-O31	1.213(5)	C58-O65	1.211(5)
Angle	***ω*, °**	**Angle**	***ω*, °**
C30-N23-C24	112.2(3)	C58-N57-C64	112.1(3)
C1-O2-C3	121.9(3)	C35-O36-C37	122.2(3)
C7-O8-C9	122.0(3)	C41-O42-C43	121.8(3)
C15-O16-C17	117.4(3)	C51-O50-C49	117.7(3)

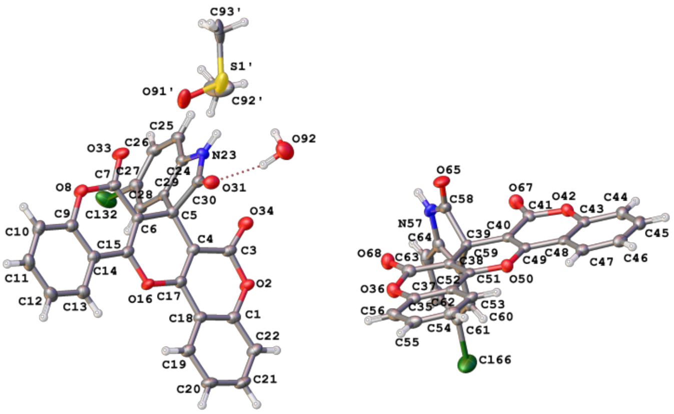

2 1

Figure 1. The molecular structure of compound **I**.

The asymmetric unit consists of two molecules of title molecule **I**, a molecule of solvent DMSO, a water molecule, and a partial water molecule's H-atoms could not be located. Molecules **1** and **2** of compound are build up from a fused pyrrole and pyran ring systems through a spiro junction at common carbon atom C5 and C39 in respectively. All atoms of DMSO solvent molecule and partial oxygen atoms are refined to a site of occupancy of 0.5000. The structural parameters, including bond distances and angles show a normal geometry, and are close to their normal geometry [27] and shows a fair amount of agreement with the related molecule ($C_{26}H_{12}ClNO_6$) which is actually a polymorphic molecule, having no crystallized solvent molecules [28].

For central pyran of molecule **1**, O16-C17, O16-C15 bond distance of 1.371(5), 1.365(5) Å and bond angle C15-O16-C17= 117.4(3)° and for molecule **2**, O50-C49 = 1.372(4), O50-C51 = 1.364(5) Å and bond angle C52-O50-C49 =117.7(3)° are in agreement with the C(sp^2)-O(sp^2) distance and angle, which are quite similar to related structure [1.366(3), 1.369(3); 1.369(3), 1.369(3)Å; 117.0(2)°, 117.3(2)°, respectively]. Whereas the bond lengths and angles for oxygen atom for chromene rings of molecule **1**, O2-C1= 1.379(5), O2-C3 =1.382(5) Å and C1-O2-C3 = 121.9(3)° of ring *A* (C1/C18/C17/C4/C3/O2); O8-C9 = 1.378(5), O8-C7 = 1.375(5) Å and C9-O8-C7 =122.0(3)° of ring *B* (C15/C14/C9/O8/C7/C6); for chromene rings of molecule **2**, O42-C43 = 1.383(5), O42-C41 =1.376(5) Å and C43-O42-C41 = 121.8(3)° of ring *C* (C52/C35/O36/C37/C38/C51), O36-C35 =1.374(5), O36-C37 =1.382(5) Å, C35-O36-C37 =122.2(3)° of ring *D* (C43/C48/C49/C40/C41/O42) indicates hetero π-electron delocalization over carbonyl groups attached to these rings. The C=O bond lengths of 1.215(5), 1.212(5), 1.202(5), 1.202(5), 1.213(5), 1.211(5) Å at C3, C7, C41, C37, C30, C58 are very close to the standard value for carbonyl group {1.210 Å; [27]}. The N23-C24, N57-C64; and N23-C30, N57-C58 bond lengths [1.393(5), 1.393(5) and 1.360(5), 1.366(5) Å, respecttively] differ from the corresponding mean values of 1.419 and 1.331 Å, respectively, as reported for γ-lactams [27], which may reflect the delocalization of electrons in this ring. In addition, around C5 and C39 in pyrrole ring, C29-C5-C30 and C58-C39-C59 [101.1(3)°, 101.3(3)°] deviate significantly from the ideal tetrahedral value of 109.4°. Whereas in pyran ring, the angles [C4-C5-C6= 107.8(3)°, C40–C39–C38 = 107.9(3)°] are signifycantly closer to similar angle of 107.5(2)°, 108.4(2)° of the related structure. The chlorine atom substituted at C27 and C61 are at 1.743(4), 1.749(4) Å of bond lengths, respectively.

In the benzene rings of the indole ring systems, the endocyclic angles at C25, C28, C63, and C60 are narrowed while those at C24, C27, C59, C64, and C61 are expanded from 120°, in accordance with the theoretical value of sp^2 hybridization. All chromene nucleus are planar [highest displacement of -0.075(4), -0.034(4), -0.049(4), -0.715(4) Å for atom C3, C7, C54, and C49, respectively]. In addition, in oxindole the small values of the highest displacement of 0.028(4), -0.032(4) for C26 and C59, respectively, shows their planar nature. The dihedral angle of 88.06(9)°, 88.23(9)° shows that the oxindole ring is almost perpendicular to the fused pyran moiety in molecules **1** and **2**, respectively. Selected bond lengths and angles for compound **I** are shown in Table 2.

Hydrogen bonded interactions between title molecule and solvent molecules are also observed. Analysis of the crystal packing showed that there exists O-H···O, N-H···O and C-H···O type of intra- and inter-molecular hydrogen bonds which plays an important role along with the weak Van der Waal's forces in stabilization of crystal structure.

Table 3. Geometry of intermolecular and intramolecular interactions for compound **I**.

D*–H···*A	***D*–H, Å**	**H···*A*, Å**	***D*···*A*, Å**	**∠(*D*–H···*A*), °**
O94-H93D···O68^{viii}	0.92	2.26	3.16(2)	168
O94-H93E···O34^{ii}	0.85	2.35	3.12(2)	150
O94-H93F···O93	0.97	2.42	2.82(2)	104
O92-H92G···O92^{i}	1.08	1.08	2.165(12)	180
O92-H92G···O91^{i}	1.08	1.86	2.930(12)	170
O91-H93G···O91'^{i}	1.09(9)	2.04(7)	2.854(1)	129(7)
O91'-H93G···O93^{i}	1.09(9)	2.44(8)	2.932(1)	106(6)
N23-H23···O91^{ii}	0.86	2.02	2.826(8)	156
N23-H23···O92^{ii}	0.86	2.15	2.869(9)	141
N57-H57···O91'^{viii}	0.86	2.13	2.905(7)	150
N57-H57···O93^{viii}	0.86	2.19	2.919(9)	143
C92-H92C···O31^{vii}	0.96	2.45	3.129(1)	127
C93-H93B···O91'^{v}	0.96	2.28	3.184(1)	157
C93-H93B···O93^{v}	0.96	2.05	2.786(1)	132
C11-H11···O36^{iv}	0.93	2.55	3.175(6)	125
C11-H11···O68^{iv}	0.93	2.56	3.465(6)	164
C13-H11···O31^{iii}	0.93	2.36	3.121(5)	139
C20-H20···O65^{v}	0.93	2.48	3.285(6)	144
C53-H53···O65^{vi}	0.93	2.59	3.386(5)	144

Symmetry codes: (*i*) 2-*x*, -*y*, 1-*z*, (*ii*) 1-*x*, 1-*y*, 1-*z*, (*iii*) -*x*, 1-*y*, 1-*z*, (*iv*) -1+*x*, *y*, *z*, (*v*) 1-*x*, -*y*, 1-*z*, (*vi*) 2-*x*, -*y*, -*z*, (*vii*) 1+*x*, -1+*y*, *z*, (*viii*) *x*, *y*, *z*.

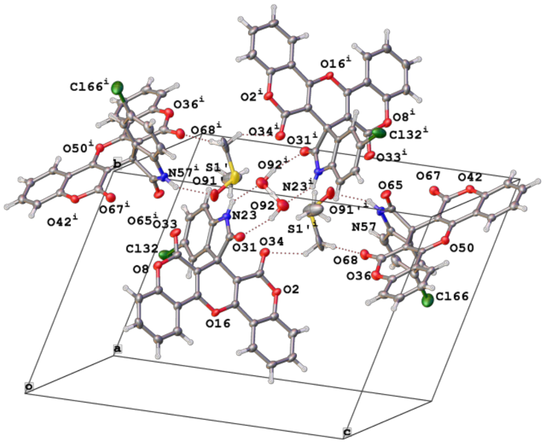

Figure 2. Molecule packing of compound **I**.

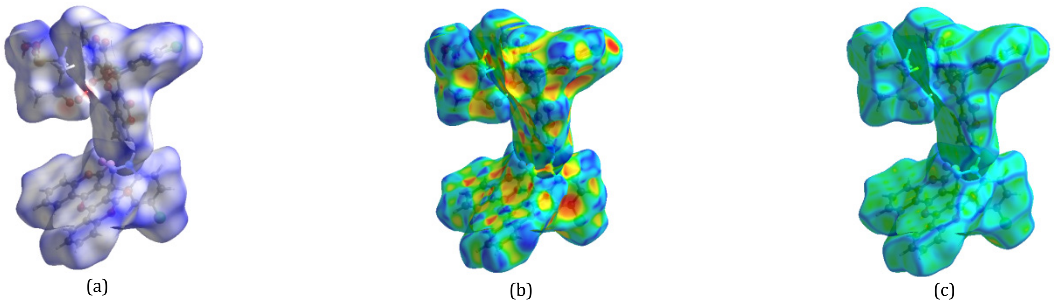

Figure 3. Hirshfeld surface: (a) d_{norm}, (b) shape index, and (c) curvature for compound **I**.

In addition, there exists halogen bonding Cl32···Cl66^{i} = 3.40(2) Å (*i*: *x*, *y*, *z*-1) which plays a decisive role in the crystal organization. The geometry of H-bond interactions is presented in Table 3, respectively. The molecular packing in the unit cell is shown in Figure 2.

3.2. Hirshfeld surface analysis

In order to carry out the Hirshfeld surface analysis and to create fingerprint plots, Crystal Explorer 17 program was used, for which the crystallographic information file (CIF) was used as input. Hirshfeld molecular surfaces are created by dividing the space in the crystal into a number of regions based on the electronic distribution of atoms along the crystal. Figure 3 shows the 3D Hirshfeld d_{norm} surfaces, the shape index and curvature for crystal **I**, which is achieved by mapping d_{norm} over the Hirshfeld surface in the range from -1.7938 to 1.2916 Å for crystal **I**. This indicates interactions between neighboring molecules.

Transparent surfaces are shown to visualize the functional groups present within the surface. In order to map d_{norm} values over the Hirshfeld surface, a red-white-blue color scheme has been used. The red-white-blue color regions symbolize closer contacts with negative d_{norm} value, the exactly comparable distance of contact at van der Waals separation with zero and longer contacts with positive d_{norm} value, respectively. The large circular red-colored spots on d_{norm} surfaces indicate hydrogen bonding contacts and other spots indicates bonding in-between other atoms. These blue and red regions indicate the positive and negative electrostatic potentials, respectively, which reveal the contribution of donor and acceptor interactions.

Table 4. Interacting residues, type of interaction, and distance of each interaction for compound **I**-1ZXM complex.

Residues involved	**Type of interaction**	**Distance (Å)**
ASN91	Hydrogen Bond	2.70270
SER149	Hydrogen Bond	1.73697
ASN150	Hydrogen Bond	2.33021
ASN150	Hydrogen Bond	1.97936
THR147	Hydrogen Bond	2.21371
ARG98	N-H⋯π	4.54276
ALA167	C-H⋯π	5.12287

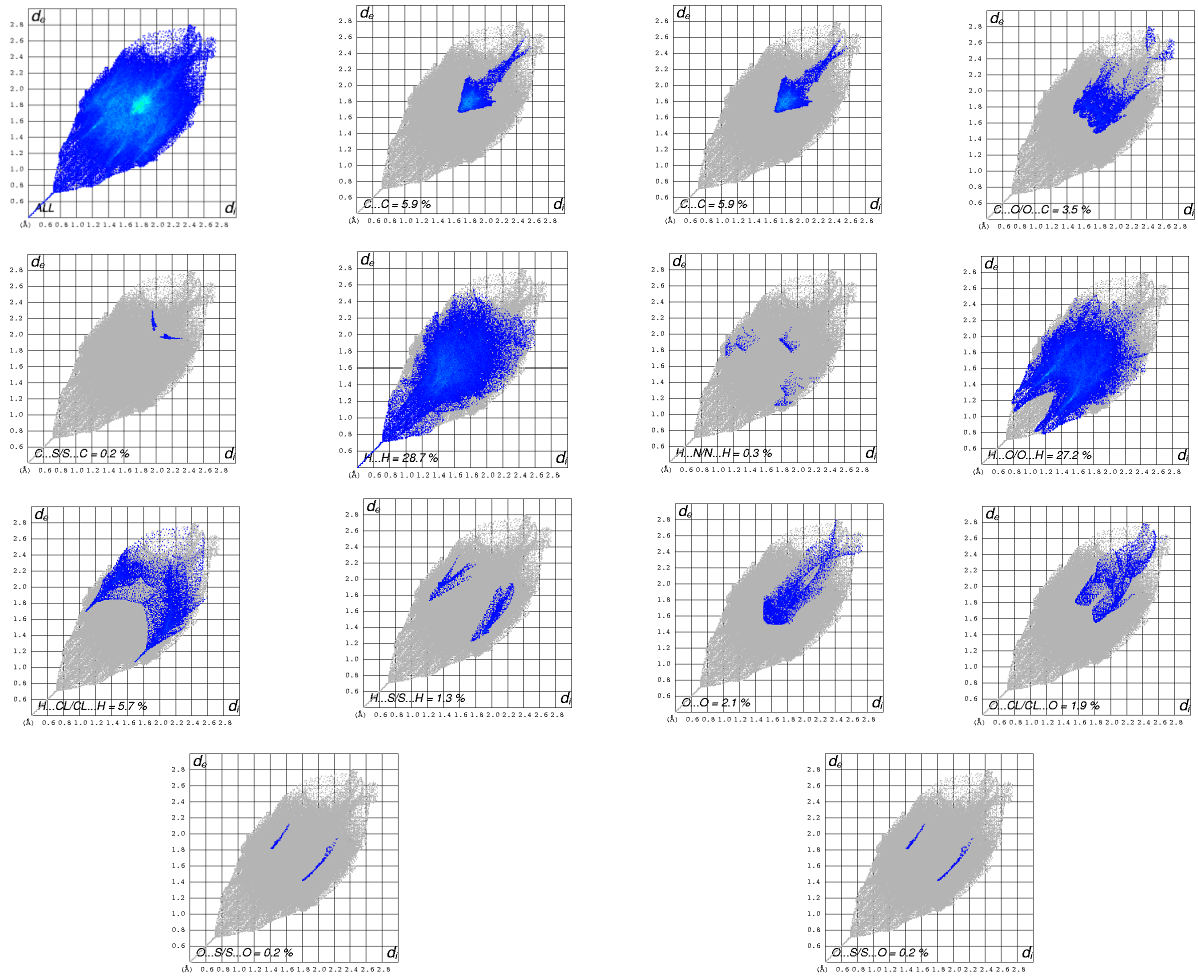

Figure 4. 2D fingerprint plots of compound **I**.

Shape index on the Hirshfeld surface can be used to recognize complementary bumps (blue) and hollows (red) and where the blue bump-shape corresponds to donor and the red hallow represents the donor of intermolecular interactions [29,30].

2D fingerprint graphs are plotted by accumulating (d_i, d_e) pairs. The coloring for each collection has been taken as a function of the fraction over surface points in compound **I**, varying blue (few points) through green (average points) to red (numerous points). A sketch of the full fingerprint is shown in grey color [31]. The corresponding 2D fingerprint plots for the Hirshfeld surfaces of compound **I**, indicating the main inter-molecular interactions with their percentage contribution to the total Hirshfeld surface area, are shown in Figure 4. Table 4 shows that H⋯H interaction is accompanied by H⋯O/O⋯H interaction with 28.7 and 27.2 %, respectively, and makes a significant contribution among all common Hirshfeld surfaces, which is clearly reflected in the middle and spikes of scattered points in 2D fingerprint plots.

3.3. In silico validation

Molecular docking explores the ways in which two molecules such as drug and a receptor fit together or dock to each other properly. The molecule is combined to a receptor for inhibition function, thus acts effectively as a drug. The docking energy obtained, gives approximate estimate of an interaction energy value, which is minimized successively. For each docked complex, nine conformations were obtained and based on the high docking energy score, the best conformation was selected. The docking result clearly shows that the molecule **I** is effectively bonded with both 1ZXM to form compound **I**-1ZXM complex with docking energy of -9.5 kcal/mol. The visual examination of the docked complex was done by evaluating the hydrogen bond interactions for compound **I**-1ZXM complex resulted in best pose to interact by hydrogen bonds with ASN91, SER149 and THR147 active site residues; along with bifurcated hydrogen bonds with active site residue ASN150. Benzene ring is involved in π-Alkyl interactions with the side chains of residue ARG98 and ALA167.

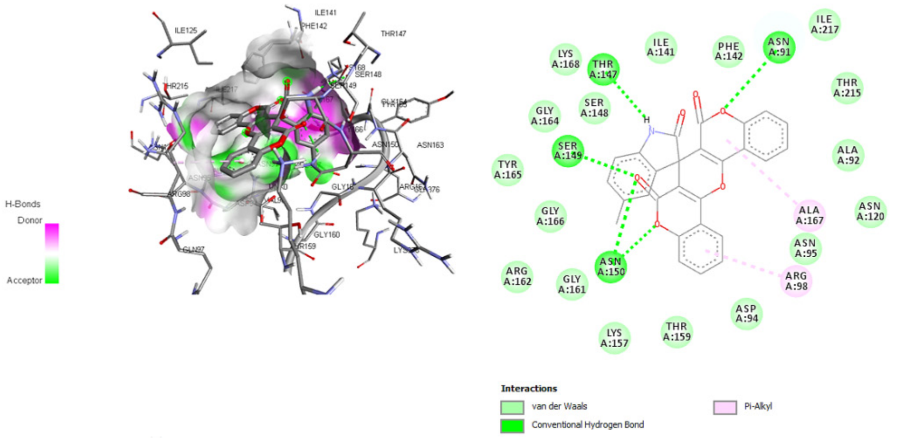

(a) (b)

Figure 5. (a) H-bond surface mapped over 3D docking modes; (b) 2D view of all the interactions between various residues and the ligand in (I)-1ZXM complex.

Table 4 contains details of the interactions present in the compound **I**-1ZXM complex. Figure 5 shows H-bond surface mapped over 3D docking modes and 2D view of all the interactions between various residues and the ligand in compound **I**-1ZXM complex.

4. Conclusions

Spiroheterocycles comprised of two or more heterocyclic skeleton are often found to possess significant pharmacological efficacies which motivated us to synthesize a spiro-oxindole fused pyrano-bis-2*H*-l-benzopyran derivative namely 5-chloro-spiro[indoline-3, 7'-pyrano[3, 2-*c*:5, 6-*c*']dichromene]-2, 6', 8'-trione. Single X-ray crystallographic studies showed the role played by solvent molecules in crystal structure stabilization although different hydrogen bond modes. Hirshfeld surface analysis helped to quantify and identify the robust synthons. The two-dimensional fingerprint plots indicated that H⋯H and H⋯O/O⋯H are the major contributors towards the inter-molecular contact interactions. From the molecular docking results of compound **I**-1ZXM complex, the occurrence of five hydrogen bonds and two π-alkyl bond confirms the potential inhibitory nature of title molecule to binding sites of human topoisomerase IIα.

Acknowledgements

Vivek Kumar Gupta is thankful to University of Jammu, Jammu, India, for financial support under Rashtriya Uchchatar Shiksha Abhiyan (RUSA) 2.0 Project. (Ref. No: RUSA/JU/2/ 2019-20/111/3588-3636).

Supporting information S

CCDC-2070425 contains the supplementary crystallographic data for this paper. These data can be obtained free of charge via https://www.ccdc.cam.ac.uk/structures/, or by e-mailing data_request@ccdc.cam.ac.uk, or by contacting The Cambridge Crystallographic Data Centre, 12 Union Road, Cambridge CB2 1EZ, UK; fax: +44(0)1223-336033.

Disclosure statement DS

Conflict of interests: The authors declare that they have no conflict of interest.
Ethical approval: All ethical guidelines have been adhered.
Sample availability: Samples of the compounds are available from the author.

CRediT authorship contribution statement CR

Conceptualization: Varun Sharma; Methodology: Aditi Sharma, Bubun Banerjee; Software: Varun Sharma; Validation: Bubun Banerjee; Formal Analysis: Vivek Kumar Gupta; Investigation: Bubun Banerjee; Resources: Vivek Kumar Gupta; Data Curation: Bubun Banerjee; Writing - Original Draft: Varun Sharma, Bubun Banerjee; Writing - Review and Editing: Vivek Kumar Gupta, Bubun Banerjee; Visualization: Vivek Kumar Gupta; Funding acquisition: Vivek Kumar Gupta; Supervision: Vivek Kumar Gupta; Project Administration: Vivek Kumar Gupta.

ORCID

Varun Sharma
https://orcid.org/0000-0003-2866-8638
Bubun Banerjee
https://orcid.org/0000-0001-7119-9377
Aditi Sharma
https://orcid.org/0000-0001-7777-0896
Vivek Kumar Gupta
https://orcid.org/0000-0003-2471-5943

References

[1]. Banerjee, B.; Kaur, G.; Kaur, N. *Curr. Org. Chem.* **2021**, *25* (1), 209–222.
[2]. Kaur, G.; Moudgil, R.; Shamim, M.; Gupta, V. K.; Banerjee, B. *Synth. Commun.* **2021**, *51* (7), 1100–1120.
[3]. Brahmachari, G.; Banerjee, B. *ACS Sustain. Chem. Eng.* **2014**, *2* (3), 411–422.
[4]. Kaur, G.; Singh, D.; Singh, A.; Banerjee, B. *Synth. Commun.* **2021**, *51* (7), 1045–1057.
[5]. Sharma, V.; Kaur, G.; Singh, A.; Banerjee, B.; Gupta, V. K. *Crystallogr. Rep.* **2020**, *65* (7), 1195–1201.
[6]. Parthasarathy, K.; Praveen, C.; Saranraj, K.; Balachandran, C.; Kumar, P. S. *Med. Chem. Res.* **2016**, *25* (10), 2155–2170.
[7]. Sharma, V.; Banerjee, B.; Kaur, G.; Gupta, V. K. *Eur. J. Chem.* **2021**, *12* (2), 187–191.
[8]. Kaur, G.; Singh, A.; Kaur, N.; Banerjee, B. *Synth. Commun.* **2021**, *51* (7), 1121–1131.
[9]. Banik, B. K.; Banerjee, B.; Kaur, G.; Saroch, S.; Kumar, R. *Molecules* **2020**, *25* (24), 5918.
[10]. Banerjee, B. *Curr. Org. Chem.* **2018**, *22* (3), 208–233.
[11]. Banerjee, B.; Bhardwaj, V.; Kaur, A.; Kaur, G.; Singh, A. *Curr. Org. Chem.* **2020**, *23* (28), 3191–3205.
[12]. Banerjee, B.; Brahmachari, G. *J. Chem. Res.* **2014**, *38* (12), 745–750.
[13]. Brahmachari, G.; Banerjee, B. *ACS Sustain. Chem. Eng.* **2014**, *2* (12), 2802–2812.
[14]. Brahmachari, G.; Banerjee, B. *Asian J. Org. Chem.* **2016**, *5* (2), 271–286.
[15]. Kaur, G.; Singh, A.; Bala, K.; Devi, M.; Kumari, A.; Devi, S.; Devi, R.; Gupta, V. K.; Banerjee, B. *Curr. Org. Chem.* **2019**, *23* (16), 1778–1788.
[16]. Singh, A.; Kaur, G.; Kaur, A.; Gupta, V. K.; Banerjee, B. *Curr. Green Chem.* **2020**, *7* (1), 128–140.

[17]. Kaur, G.; Shamim, M.; Bhardwaj, V.; Gupta, V. K.; Banerjee, B. *Synth. Commun.* **2020**, *50* (10), 1545–1560.
[18]. Kaur, G.; Kumar, R.; Saroch, S.; Gupta, V. K.; Banerjee, B. *Curr. Organocatalysis* **2021**, *8* (1), 147–159.
[19]. Sheldrick, G. M. *Acta Crystallogr. A Found. Adv.* **2015**, *71* (Pt 1), 3–8.
[20]. Farrugia, L. J. *J. Appl. Crystallogr.* **1997**, *30* (5), 565–565.
[21]. Nardelli, M. *J. Appl. Crystallogr.* **1995**, *28* (5), 659–659.
[22]. Spek, A. L. *Acta Crystallogr. D Biol. Crystallogr.* **2009**, *65* (Pt 2), 148–155.
[23]. Spackman, P. R.; Turner, M. J.; McKinnon, J. J.; Wolff, S. K.; Grimwood, D. J.; Jayatilaka, D.; Spackman, M. A. *J. Appl. Crystallogr.* **2021**, *54* (Pt 3), 1006–1011.
[24]. Wei, H.; Ruthenburg, A. J.; Bechis, S. K.; Verdine, G. L. *J. Biol. Chem.* **2005**, *280* (44), 37041–37047.
[25]. Discovery Studio: Dassault Systems BIOVIA, Discovery Studio Modelling Environment, Release 4.5, Dassault Systems: San Diego, 2015. From
[26]. Farrugia, L. J. *J. Appl. Crystallogr.* **2012**, *45* (4), 849–854.
[27]. Allen, F. H.; Kennard, O.; Watson, D. G.; Brammer, L.; Orpen, A. G.; Taylor, R. *J. Chem. Soc., Perkin Trans. 2* **1987**, *12*, S1–S19.
[28]. Almansour, A. I.; Kumar, R. S.; Arumugam, N.; Kanagalaksmi, S.; Suresh, J. *Acta Crystallogr. Sect. E Struct. Rep. Online* **2012**, *68* (Pt 4), o1172.
[29]. Spackman, M. A.; Jayatilaka, D. *CrystEngComm* **2009**, *11* (1), 19–32.
[30]. Miller, G. J. *Angew. Chem. Weinheim Bergstr. Ger.* **1989**, *101* (11), 1570–1571.
[31]. Hoffmann, R. *Solids and Surfaces: A Chemist's View of Bonding in Extended Structures*; VCH, 1988.
[32]. McKinnon, J. J.; Mitchell, A. S.; Spackman, M. A. *Chemistry* **1998**, *4* (11), 2136–2141.